Talanta 83 (2011) 930–936

Contents lists available at ScienceDirect

Talanta

journal homepage: www.elsevier.com/locate/talanta

Toluidine blue adsorbed on alcohol dehydrogenase modified glassy carbon electrode for voltammetric determination of ethanol

Arun Prakash Periasamy, Yogeswaran Umasankar, Shen-Ming Chen*

Department of Chemical Engineering and Biotechnology, National Taipei University of Technology, No. 1, Section 3, Chung-Hsiao East Road, Taipei 106, Taiwan, ROC

ARTICLE INFO

Article history:
Received 26 August 2010
Received in revised form 26 October 2010
Accepted 29 October 2010
Available online 4 November 2010

Keywords:
Alcohol dehydrogenase
Toludine blue O
Nafion
Differential pulse voltammetry
Ethanol
Electrocatalysis

ABSTRACT

A novel toluidine blue O (TBO) adsorbed alcohol dehydrogenase (ADH) biocomposite film have been prepared through simple adsorption technique with the help of electrostatic interaction between oppositely charged layers. Nafion (NF) coating was made on top of the biocomposite film modified glassy carbon electrode (GCE) to protect ADH from leaching. The fabricated ADH/TBO/NF biocomposite electrode remains highly stable in the pH range from 4 to 13. More facile electron transfer process occurs at ADH/TBO/NF biocomposite than at TBO/NF film, which is obvious from the six folds increase in k_s value. Maximum surface coverage concentration (Γ) of TBO is noticed at ADH/TBO/NF film, which is 82% higher than at TBO/NF and 15% higher than at ADH/TBO film modified GCEs. Electrochemical impedance spectroscopy studies reveal that ADH has been well immobilized in the biocomposite film. Scanning electron microscopy studies confirm the discriminate surface morphology of various components present in the biocomposite film. Cyclic voltammetry studies validate that ADH/TBO/NF biocomposite film exhibits excellent electrocatalytic activity for ethanol oxidation at low over potential ($I_{pa} = -0.14$ V). The same studies show biocomposite film possesses a good sensitivity of 7.91 $\mu A\,M^{-1}\,cm^{-2}$ for ethanol determination. This above sensitivity value is 17.40% higher than the sensitivity obtained for TBO/NF film (6.74 $\mu A\,M^{-1}\,cm^{-2}$). Further, using differential pulse voltammetry, a sensitivity of 1.70 $\mu A\,M^{-1}\,cm^{-2}$ has been achieved for ADH/TBO/NF biocomposite film.

1. Introduction

The utilization of ethanol in various food and beverage industries necessitates the rapid and selective determination of ethanol present in food products [1,2]. Nevertheless, most of the standard methods used for ethanol determination such as distillation and gas chromatography techniques are laborious and time consuming one [3,4]. Owing to the recent advancements in the field of biosensors, enzyme based biosensors have been successfully employed for simple and fast determination of ethanol [5–7]. The two kinds of enzymes majorly used for the construction of ethanol biosensors are alcohol dehydrogenase (ADH) and alcohol oxidase (AOD). AOD based ethanol biosensors depend on the principle that either decrease in oxygen or increase in hydrogen peroxide will be measured from an AOD catalysed ethanol reaction [8]. Several AOD based ethanol biosensors have been successfully developed [7,9–11]. However ADH based ethanol biosensors have received much interest, because irreversible oxidation of ethanol occurs in presence of both ADH and its cofactor nicotinamide adenine dinucleotide (NAD^+) at their close proximity [8]. In the past decade various immobilization matrices and diverse strategies have been practiced to immobilize ADH on various electrode surfaces. In particular, the developed matrices are ferrocene encapsulated ormosils [12], polyethylene glycol [13], colloidal gold [14], conducting polymers [15,16], redox polymers [17] and multi-walled carbon nanotubes composite films [18–20]. Attempts have also been made to design a disposable ethanol sensor using polystyrene modified screen printed carbon electrode as the ADH immobilizing matrix [21].

Though these above approaches lead to rapid determination of ethanol, due to the oxidation of enzymatically generated nicotinamide adenine dinucleotide (NADH) at very high over potentials, these biosensors experience serious electrode surface fouling [22–24]. This ultimately leads to poor stability of biosensor which in turn slows down the electron shuttling between the enzyme and transducer surface. To overcome this electrode surface fouling problem Grundig et al. included redox mediators along with ADH, which significantly decreased the over potential of NADH oxidation [22]. Similarly, using acetophenone as a redox mediator Yuan et al. achieved 97% current efficiency for the reduction of NAD^+ to NADH at ADH modified electrode [25]. Further, with the inclusion of an oil-soluble mediator (7-dimethylamine-2-methyl-3-β-naphtamido-phenothiazinium chloride) Yao et al. noticed significant improvement in the stability of ADH/poly ethylene gly-

* Corresponding author. Tel.: +886 2270 17147; fax: +886 2270 25238.
E-mail address: smchen78@ms15.hinet.net (S.-M. Chen).

0039-9140/$ – see front matter © 2010 Elsevier B.V. All rights reserved.
doi:10.1016/j.talanta.2010.10.058

col modified carbon paste electrode [13]. Several other mediators including organo metallic ferrocene derivatives [26], redox dyes such as meldola blue [27,28], toludine blue O (TBO) [29], nile blue [30] and thionine [31] have been successfully employed in the fabrication of ADH based ethanol biosensors. These above studies ultimately reveal that the redox mediator acts as a conduit and significantly promotes the facile electron shuttling between immobilized ADH and the transducer and thereby lowers the oxidation potential of NADH and ethanol.

The redox mediators mentioned above possess electrostatic interactions between their oppositely charged materials. These electrostatic interactions behave as chief driving forces for the formation of well stable protein with redox mediator composite films [32]. Peng et al. successfully investigated the electrostatic interactions between the positively charged TBO and negatively charged protein (heparin) using voltammetry [33]. Similar approach have been practiced by Li et al. and Perinotto et al. for TBO with horseradish peroxidase, and poly(amido amine) with ADH respectively [34,35]. Because of these above advantages of redox mediators and ADH, in our studies we employed TBO adsorbed ADH biocomposite film for the ethanol determination. The prepared TBO adsorbed ADH biocomposite film decreases the over potential of ethanol oxidation also. In detail, TBO adsorption on ADH film modified glassy carbon electrode (GCE) involves electrostatic interaction between the negatively charged ADH [36,37] and positively charged TBO molecules. The significance of this film preparation is that TBO has been adsorbed over ADH modified GCE without any cross linking agents or complex matrices. The presence of TBO in the biocomposite film helps to achieve rapid electron transfer between ADH and the electrode surface. To improve the stability and protect the leaching of ADH and TBO, Nafion (NF) has been coated over the modified electrode. The entire adsorption process has been successfully monitored using cyclic voltammetry (CV).

2. Experimental

2.1. Reagents

ADH from *Saccharomyces cerevisiae* (332 U mg^{-1} protein) and NAD^+ from yeast were purchased from Sigma–Aldrich. Toludine blue was purchased from Chroma-gesellschaft and used without further purification. 5 wt% NF perfluorinated ion exchange resin from Aldrich and 95% pure ethanol from Shimakyu's pure chemicals were used as received. All other chemicals used in this study were of Analar grade. 0.1 M pH 6.5 phosphate buffer solution (PBS) was prepared using 0.1 M Na_2HPO_4 and NaH_2PO_4 solutions. All reagents were prepared with doubly distilled water. Prior to each experiment pre-purified N_2 gas was passed through the buffer solutions for 10 min.

2.2. Apparatus

CV studies were performed using a conventional three electrode system attached with CHI405 electrochemical work station. GCE with an electrode surface area of 0.079 cm^2 was used as working electrode and Pt wire with 0.5 mm diameter was used as a counter electrode. All the potentials mentioned in this work were referred with respect to standard Ag/AgCl reference electrode. IM6ex ZAHNER (Kroanch, Germany) was used for electrochemical impedance spectroscopy (EIS) studies. Surface morphological studies were carried out using Hitachi S-3000 H scanning electron microscope (SEM). CHI-750 potentiostat was used for differential pulse voltammetry (DPV) studies.

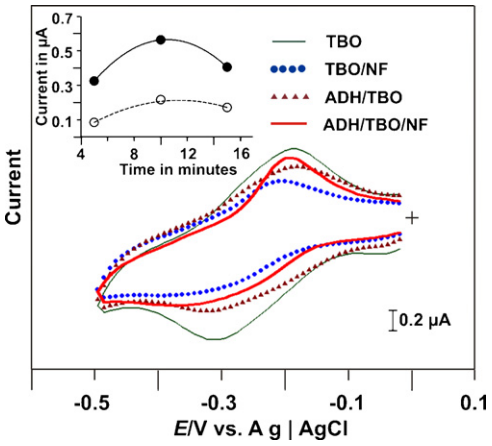

Fig. 1. Cyclic voltammograms of TBO, TBO/NF, ADH/TBO and ADH/TBO/NF modified GCEs in N_2 saturated PBS at the scan rate of 20 mV s^{-1}. Inset plot shows the different TBO adsorption time in min vs. cathodic peak current for TBO (filled dot) and ADH/TBO/NF (unfilled dot) films.

2.3. Fabrication of ADH/TBO/NF biocomposite film

Initially, 2 mg ml^{-1} ADH and 5 mM TBO solutions were prepared separately in PBS. 0.5 wt% NF solution was prepared as we reported earlier [38]. Prior to the biocomposite film fabrication, GCE surface was polished to a mirror finish on a Buehler polishing kit using 0.05 μm alumina powder. The polished GCE surface was washed and ultrasonicated with doubly distilled water and dried in air. The cleaned GCE was then utilized for the fabrication of ADH/TBO/NF biocomposite film. The biocomposite film fabrication procedure involves three steps. (i) A negatively charged ADH film was fabricated above the clean GCE surface by drop casting 6 μl of ADH solution and then drying at 25 °C in an air oven. (ii) Above the negative layer, a positively charged thin TBO film was adsorbed by immersing ADH modified GCE into 5 mM TBO solution for 10 min. After the adsorption of TBO on ADH/GCE, the modified electrode surface was washed twice with distilled water to remove the loosely adsorbed TBO molecules. (iii) To prevent further leaching of ADH and TBO molecules a negatively charged NF layer was formed over the positively charged TBO film. About 2 μl of 0.5 wt% NF solution was drop casted and dried at 25 °C in an air oven. As reported earlier, TBO molecules possess both positively charged tertiary amine group, $-NH(CH_3)_2$ and the hydrophic side chain [39]. The $-NH(CH_3)_2$ group present in TBO undergoes strong electrostatic interactions with the negatively charged $-SO_3^-$ groups present in the NF polymer backbone chain. Thus NF coating prevents the leaching of TBO molecules, which improves the stability of the ADH/TBO/NF biocomposite film. The prepared ADH/TBO/NF biocomposite film modified GCE was stored at 4 °C when not in use and used for the electrocatalytic oxidation of ethanol.

3. Results and discussions

3.1. CV studies of different film modified electrodes

The TBO adsorption time has been optimized at both TBO and ADH/TBO/NF modified GCEs using CV studies (see Fig. 1 inset). The results show that both films exhibit maximum peak current for 10 min dipping time in TBO solution. However, after 10 min the peak current decreases notably at these films which indicate that TBO adsorption have reached its saturation level. The reason for this could be due to the increased steric repulsion between the TBO molecules as reported in literature [40]. Hence, the optimum TBO adsorption time is 10 min and it has been used throughout

this work. Further, the redox behavior of TBO, TBO/NF, ADH/TBO and ADH/TBO/NF modified GCEs in N_2 saturated PBS were investigated using CV technique (Fig. 1). The potential range used for the CV studies was from 0 to −0.5 V. It is clear from Fig. 1 that TBO modified GCE exhibits a pair of well defined quasi reversible redox couple with maximum peak current at E_{pa} = −176.8 mV and E_{pc} = −328.9 mV respectively. Although, TBO/NF film exhibits similar redox couple at E_{pa} = −187.2 mV and E_{pc} = −403.0 mV, its I_{pa} value is lower than TBO film. Similarly, the I_{pa} value observed for ADH/TBO/NF biocomposite film is slightly lower than the I_{pa} value of TBO film (see Table S1 of supplementary data). Interestingly, the I_{pa} value of biocomposite film is higher than other films investigated in this work (except only TBO). This result indicates that more number of active TBO reduced species have been formed at ADH/TBO/NF film which could facilitate NADH oxidation. On the other hand, the reason for the less pronounced reduction reaction at the ADH/TBO/NF film is due to the interaction of oxidized TBO species with ADH. The formal potential ($E^{0'}$) for the TBO redox couple in ADH/TBO/NF biocomposite film is −0.24 V.

The amount of TBO present on different electrode surfaces has been given as surface coverage concentration values (Γ) in supplementary data (Table S2 of supplementary data). From the above mentioned table, it is obvious that TBO/GCE have maximum Γ value. However, ADH/TBO/NF biocomposite film possesses higher surface coverage than other two films. Where, the Γ value of TBO at ADH/TBO/NF film is 82% higher than TBO/NF and 15% higher than ADH/TBO films. This shows that the ADH facilitates the adsorption of TBO. In addition, using CV studies, the influence of scan rate on the peak currents (I_{pa} and I_{pc}) have also been studied at TBO/NF and ADH/TBO/NF modified electrodes (figure not shown). The results show that the I_{pa} and I_{pc} exhibits linear dependence over the scan rates between 20 and 280 mV s^{-1} for both TBO/NF and ADH/TBO/NF films. This indicates that the electrode processes are surface confined. From these different scan rate results, the electron transfer rate constant (k_s) for TBO and ADH/TBO/NF films have been calculated using Laviron equation [41].

$$\log k_s = \alpha \log(1-\alpha) + (1-\alpha)\log\alpha - \log\left(\frac{RT}{nF\nu}\right) - \alpha(1-\alpha)\frac{nF\Delta Ep}{2.3\,RT} \quad (1)$$

where R is the gas constant (8.314), T is the room temperature (298.15) and ΔE_p is the peak separation of the TBO redox couple. Here, α value has been assumed as ≈0.5 and the number of electrons transferred for TBO reaction is two. The k_s values are 0.02 and 0.12 s^{-1} for TBO/NF and ADH/TBO/NF modified GCEs respectively. The k_s value observed at ADH/TBO/NF film is six folds higher than that of TBO/NF film and it could be attributed to the presence of ADH on the GCE surface. These k_s values show that 51 μg cm^{-2} of ADH increases k_s value by six folds. The enhancement in the k_s value at ADH/TBO/NF biocomposite film validates an efficient electron transfer process. Perhaps, the enhancement may be due to the hydrophobic nature of GCE surface [42] which orientates the ADH in a suitable configuration and accordingly much closer contact have been established between the prosthetic group of ADH and the electrode surface. This result is in accordance with the earlier report by Schuhmann et al. in which they revealed an efficient electron transfer between quinohemo–protein ADH (QH–ADH) and the bare Au electrode surface [43]. They confirmed from their studies that efficient electron transfer must be due to the much closer contact between the heme centre of Q–ADH and the Au electrode surface which was established by the hydrophobic nature of Au electrode which orientates the protein in a suitable configuration. In the present study, since ADH has been anchored well beneath the positively charged TBO layer a much better contact have been made between the prosthetic group of ADH and the underlying electrode surface. Furthermore, as a result of the strong electrostatic interactions between the negatively charged ADH and positively charged TBO molecules, the prosthetic group of ADH have been surrounded by sufficient number of TBO molecules which mediates a fast electron transfer process.

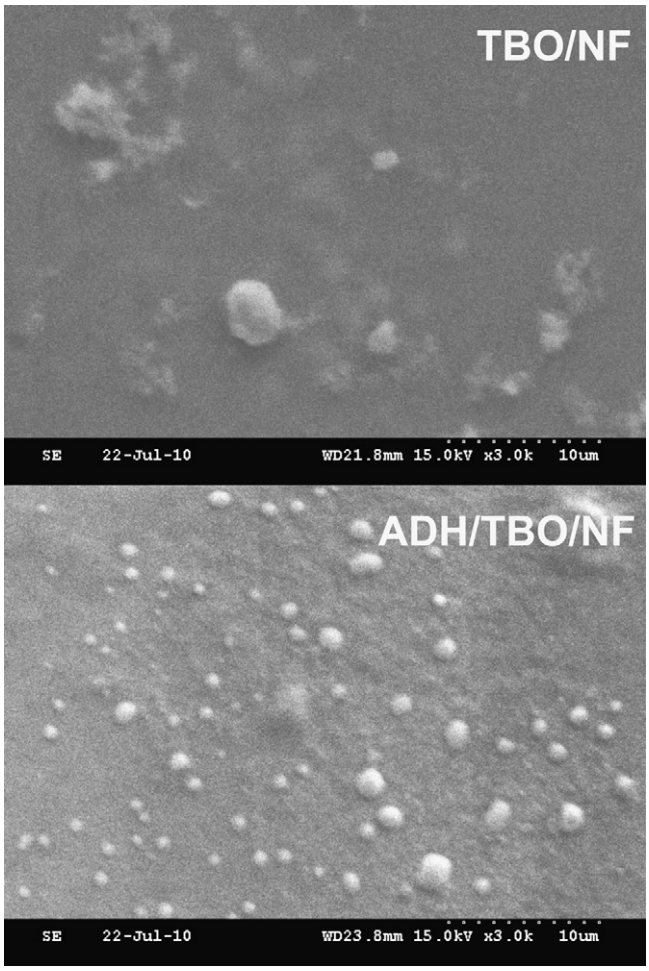

Fig. 2. SEM images of TBO/NF and ADH/TBO/NF modified GCEs.

3.2. Surface morphological characterization using SEM

Fig. 2 shows the top view SEM images of TBO/NF and ADH/TBO/NF film modified GCEs. In the TBO/NF film, only few bright, spherical shaped NF coated TBO molecules are clearly seen in the midst of TBO clusters. These TBO clusters would have been formed due to the association of several small TBO granules. This result reveals the uneven surface morphology of TBO/NF film. In contrast, the ADH/TBO/NF film possesses more uniform surface morphology. Several spherical shaped TBO granules have been uniformly distributed through out the ADH film surface. All the ADH and TBO molecules have been collectively covered well by the NF film. It is noteworthy here that the strong electrostatic interactions offered by ADH towards TBO facilitate the efficient TBO adsorption. For comparison, the SEM images of ADH, NF, ADH/TBO and TBO film modified GCEs are given in supplementary data (Fig. S1 of supplementary data). Fig. S1(a–d) shows the discriminate surface morphology between all the above said films. Interestingly, the ADH film possesses uniform distribution of several small beads like structures, while NF film possesses a very thin film surface morphology (see Fig. S1a and b). It is understandable from Fig. S1(c) and (d) that more amount of TBO has been adsorbed at

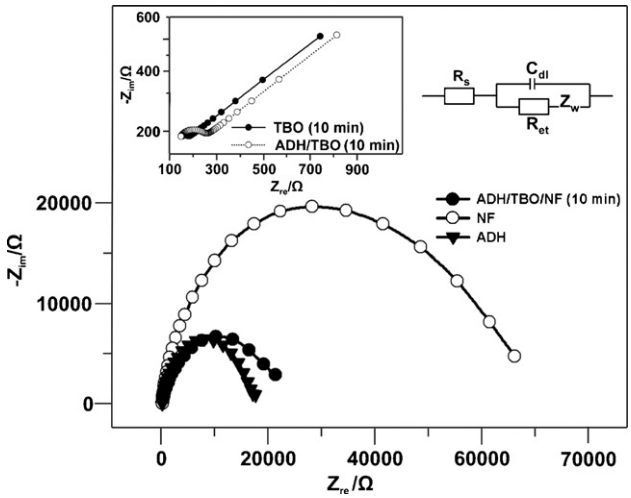

Fig. 3. EIS of ADH, NF and ADH/TBO/NF film modified GCEs in PBS containing 5 mM $Fe(CN)_6^{3-}/Fe(CN)_6^{4-}$. Amplitude: 5 mV, frequency: 0.1 Hz–100 kHz. The inset at the upper left is the EIS of TBO and ADH/TBO film modified GCEs recorded under similar experimental conditions as that of the other films shown in Fig. 3. The optimized TBO adsorption time, 10 min has been given within brackets in the legend of upper left inset. Inset at the upper right is the Randles equivalence circuit model for all the above modified GCEs.

ADH/TBO than TBO film. SEM results thus ultimately reveals that ADH modified GCE surface is more efficient for TBO adsorption.

3.3. Influence of pH at the biocomposite film modified GCE

The influence of pH on the electrocatalytic activity of ADH/TBO/NF biocomposite film modified GCE has been investigated in different buffer solutions (pH 1–13) containing 25 mM NAD^+ and 0.5 M ethanol (within the linear range). The results are shown in Fig. S2 (see supplementary data). It is clear from Fig. S2 that the biocomposite film exhibits well defined oxidation peak for ethanol in near neutral (pH 6.5) and alkaline media (pH 11 and 13) which shows its good electrocatalytic activity. On the other hand, in slightly alkaline medium (pH 8.5), the biocomposite film exhibits a weak electrocatalytic response with less oxidation peak current. Likewise, in acidic media (pH 1 and 4) the oxidation peak currents decreased further. Since the enzyme activity is appreciable in pH 6.5, we utilized pH 6.5 PBS for all the electrocatalytic experiments. Fig. S2 inset shows the linear dependence of E_{pa}, E_{pc} and $E^{0\prime}$ with pH. The plot of $E^{0\prime}$ vs. pH has the slope value of −48 mV pH^{-1}. This slope value shows that the biocomposite electrode exhibit an equal number of proton and electron transfer process according to the Nernstian equation.

3.4. EIS studies

EIS is a valuable tool to probe the interfacial changes occurring at the electrode surface due to the bio recognition events [44]. From EIS data, the value of equivalence circuit parameters have been calculated, which in turn revealed the electrochemical characteristics of ADH, TBO and NF immobilized on GCE. Fig. 3 shows the real and imaginary parts of impedance spectra represented as Nyquist plots (Z_{im} vs. Z_{re}) for NF, ADH and ADH/TBO/NF film modified GCEs. The electrolyte used for these experiments is PBS containing 5 mM $Fe(CN)_6^{3-/4-}$. It is clear from these Nyquist plots that all the above said films exhibit semicircles with variable diameters in the frequency range between 0.1 Hz and 100 kHz. The semicircle portion observed at higher frequencies corresponds to the electron-transfer-limited process and the diameter of the semicircle corresponds to the interfacial electron-transfer resistance (R_{et}). Likewise, the linear part of the spectrum is the characteristic of the lower frequency range and represents the diffusional-limited process [44,45]. In these results, a large semicircle with maximum R_{et} value (4,6200 Ω) has been observed at only NF film which corroborates a high electron transfer resistance. The great hindrance to electron transfer observed at NF film is due to the repulsion between the negatively charged SO^{3-} groups of NF polymer back bone and the negatively charged Fe $(CN)_6^{3-}$ ions, which prevents the later from approaching the electrode surface. Conversely, more rapid electron transfer processes occurs at ADH and ADH/TBO/NF films which is apparent from their depressed semicircle diameters and lesser R_{et} values such as 9309 Ω and 16,200 Ω respectively. The higher R_{et} value observed at ADH/TBO/NF than ADH film indicates that ADH has been well immobilized at the comoposite film. In addition, the R_{et} value observed at the ADH/TBO/NF film is much higher than that of TBO (R_{et} = 148.5 Ω) and ADH/TBO films (R_{et} = 269.3 Ω). Here it is noteworthy that the presence of NF film leads to significant charge transfer enhancement at the ADH/TBO/NF film. The corresponding Nyquist plots of TBO and ADH/TBO films are shown in Fig. 3 upper left inset. Even though the above results show that NF coating enhances the charge transfer resistance, it significantly improves the stability of ADH and TBO on the composite electrode. Briefly, the order of the charge transfer resistance for various film modified GCEs is NF > ADH/TBO/NF > ADH > ADH/TBO > TBO.

3.5. Electrocatalysis (CV and DPV) studies for ethanol determination

Fig. 4(A) shows the cyclic voltammograms obtained at ADH/TBO/NF biocomposite film in N_2 saturated PBS with different ethanol concentrations (0.01–1.02 M) and 25 mM NAD^+. Cyclic voltammograms have been recorded at the scan rate of 20 mV s^{-1} in the potential range between 0 and −0.5 V vs. Ag/AgCl reference electrode. Interestingly, the bare GCE shows no response even in the presence of highest ethanol concentration (1.02 M) even though the potential was swept towards more positive potential (0.1 V) as shown in Fig. 4A(a′). Whereas, a significant increase in catalytic oxidation peak (−0.14 V) has been observed at ADH/TBO/NF film even for 0.01 M ethanol (see Fig. 4A(a)). After this, for each ethanol concentration additions the oxidation peak current increases and it was linear up to 1.02 M ethanol (see Fig. 4A(b–j)). The remarkable increase in the anodic peak current at the composite film is due to the oxidation of NADH produced in the enzymatic reaction and it has been greatly facilitated in the presence of TBO. In addition, in the presence of very high concentration of ethanol (1.02 M), ADH/TBO/NF film shows much higher oxidation peak current than TBO/NF film. Interestingly, the oxidation peak potential of NADH (ethanol addition) at ADH/TBO/NF film (−0.14 V) is found to be 30 mV lower than TBO/NF film (−0.17). This demonstrates that, electrocatalysis of NADH (ethanol addition) takes place efficiently at ADH/TBO/NF film than TBO/NF film. Where, both the increase in peak current and decrease in over potential are considered as electrocatalysis [46]. The detailed mechanism of electrocatalytic detection of ethanol at the ADH/TBO/NF biocomposite electrode is schematically given in Fig. S3 (see supplementary data). The linear dependence of anodic peak currents of ADH/TBO/NF and TBO/NF films with various ethanol concentrations are shown in Fig. 4(A) inset. From the inset, the sensitivity and correlation coefficient values obtained for ADH/TBO/NF film are 7.91 μA M^{-1} cm^{-2} and 0.9992. While the sensitivity and correlation coefficient values for TBO/NF film are 6.74 μA M^{-1} cm^{-2} and 0.9938 respectively. Thus ADH/TBO/NF film possesses 17.40% higher sensitivity than TBO/NF film. From electrocatalytic CV studies it is evident that maximum catalytic activity with higher sensitivity has been achieved at ADH/TBO/NF biocomposite film than at TBO/NF film.

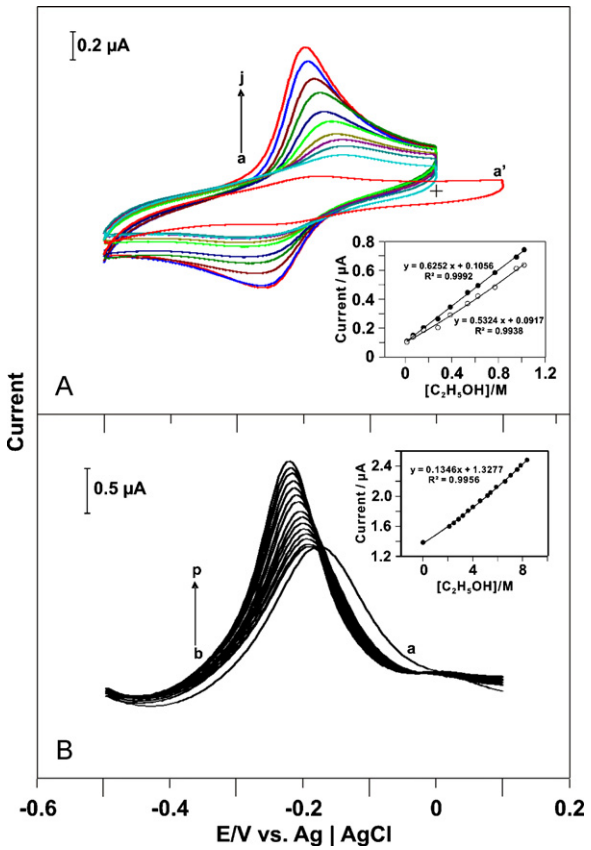

Fig. 4. (A) Cyclic voltammograms obtained at ADH/TBO/NF biocomposite film modified GCE at the scan rate of 20 mV s^{-1} in the presence of 0.01–1.02 M ethanol (a–j). (a′) Represents the cyclic voltammogram obtained at bare GCE in presence of highest (1.02 M) ethanol concentration. Supporting electrolyte: N_2 saturated PBS containing 25 mM NAD^+. Inset plot shows the linear dependence of peak current vs. [ethanol] M^{-1} for ADH/TBO/NF (filled dot) and ADH/TBO (unfilled dot) film modified GCEs (B) DPV curves obtained at ADH/TBO/NF biocomposite film in the absence (a) and presence of 2.11–8.37 M ethanol (b–p). Supporting electrolyte: N_2 saturated PBS containing 25 mM NAD^+. Inset plot shows the linear dependence of peak current vs. [ethanol] M^{-1} for ADH/TBO/NF (filled dot) film modified GCE.

Fig. 4B(a) represents the DPV curve recorded at ADH/TBO/NF biocomposite film in N_2 saturated PBS in the absence of ethanol. Similarly, Fig. 4(B)(b–p) shows the DPV curves recorded at ADH/TBO/NF film in N_2 saturated PBS with different ethanol concentrations (2.11–8.37 M) and 25 mM NAD^+. After each successive ethanol addition, pre-purified N_2 gas was purged into PBS for 45 s before recording the next cyclic voltammogram. From the corresponding DPV curves, the I_{pa} values were obtained and plotted against ethanol concentration as shown in Fig. 4(B) inset. The inset plot shows that oxidation peak current of ADH/TBO/NF film increases linearly from 2.48 to 6.61 M ethanol. The sensitivity and the correlation coefficient values are 1.70 μA M cm^{-2} and 0.9956 respectively. In general, DPV results reveal that ADH/TBO/NF film is efficient for ethanol determination.

3.6. Electrocatalysis of ethanol by TBO adsorbed "NAD^+ co-immobilized ADH"

As the future aspect of this work, we endeavor also to improve the electrocatalytic efficiency and working linear range of the developed ethanol biosensor. In our alternative approach, instead of adding the cofactor NAD^+ into buffer solution we co-immobilized NAD^+ along with ADH. For this purpose, 25 μM NAD^+ was added in to 2 mg ml^{-1} ADH stock solution. The whole mixture was gently stirred for few min and stored at 4 °C. About 6 μl of ADH/NAD^+ solution was taken with a micro syringe and carefully drop casted above the clean GCE surface and dried at 25 °C. This results in the formation of a negatively charged ADH/NAD^+ film on GCE. Later, positively charged TBO and negatively charged NF layers were sequentially formed over ADH/NAD^+ film modified GCE following the similar experimental procedure explained in Section 2.3. Hereafter the NAD^+ co-immobilized film will be mentioned as ADH–NAD/TBO/NF film. The electrocatalytic activity of the prepared ADH–NAD/TBO/NF film towards ethanol has been investigated using DPV technique. The results are shown in Fig. S4 (see supplementary data). It is clear that the ADH–NAD/TBO/NF film exhibits excellent electrocatalytic response towards 283–856 mM ethanol. The sensitivity and correlation coefficient are 0.02 μA mM^{-1} cm^{-2} and 0.9732 respectively. The limit of detection is 29 mM of ethanol. DPV results reveal that ADH–NAD/TBO/NF film possesses excellent catalytic activity towards ethanol than ADH/TBO/NF film. The reason for the promising catalytic activity of ADH–NAD/TBO/NF film could be the easy accessibility of NAD^+ by ADH since it was co-immobilized on the electrode surface. In contrast, in the case of ADH/TBO/NF film since NAD^+ was added into the solution ADH could not quickly access its cofactor because the diffusion rate of NAD^+ will be much slower. This influences the electrocatalytic efficiency of the composite film towards ethanol.

On the other hand, attempts were also made to explore the maximum possible adsorption sites of TBO (T1 and T2) and NF (N1, N2 and N3) at ADH, both in the absence and presence of NAD^+. The possible adsorption sites are given in Fig. 5. The simulation has been carried out using Lamarckian genetic algorithm, where the TBO molecules were docked on ADH (absence/presence of NAD^+) and then followed by docking of NF molecules over them. The simulation conditions such as population size (50), maximum generations (3000), crossover rate (0.8), mutation rate (0.2), elitism (5), local search rate (0.06) and local search maximum steps (100) were kept

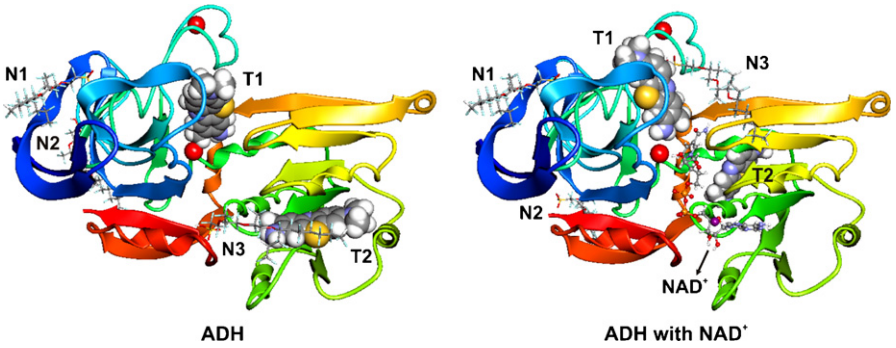

Fig. 5. Schematic representation of the possible adsorption sites of TBO (T1 and T2) and NF (N1, N2 and N3) at ADH in the absence and presence of NAD^+, given by Lamarckian genetic algorithm.

constant and the area around the binding site was maintained in the ratio of 6 × 4.86 × 4.64 nm for all the experiments. The results reveal that among numerous TBO and NF molecules used in docking experiments (not shown in figure), two TBO molecules and three NF molecules adsorbs well on ADH in the absence of NAD^+, with the minimum free energy of −10.28 (T1), −9.2 (T2), −8.17 (N1), −7.57 (N2) and −8.81 kcal mol^{-1} (N3). However in presence of NAD^+, the adsorption sites of T1, T2 and N3 have been changed, and the minimum free energy values are −10.15 (T1), −8.79 (T2), −7.39 (N1), −8.48 (N2) and −8.17 kcal mol^{-1} (N3). Comparison of free energy values between the enzyme models shows that because of steric hindrance of NAD^+, the free energy is higher in presence of NAD^+, whereas the values are low in absence of NAD^+. These lowest free energy values reveal the most probable adsorption sites of TBO and NF on ADH in the absence and presence of NAD^+ as given in Fig. 5.

3.7. Repeatability, reproducibility, stability and selectivity studies

The electrocatalysis of ethanol at ADH/TBO/NF biocomposite film has been studied in detail using DPV technique to determine the repeatability, reproducibility and selectivity of the modified GCE. The DPV experimental conditions are similar to the pervious studies mentioned in Section 3.5. The electrocatalytic experiments have been carried out twelve times for the same film modified electrode with same concentration of ethanol (1.5 M), where the ethanol has been renewed for each determination. The renewal of ethanol has been done along with the renewal of supporting electrolyte solution. The obtained I_{pa} values of ethanol from the above determinations have been plotted as the percentage of current decrease vs. number of repeated analysis of ethanol (shown in Fig. S5 of supplementary data). These plots show that there is no decrease in the I_{pa} of ethanol up to five determinations, however after five determinations the I_{pa} of ethanol gradually decreases. These results reveal that the ADH/TBO/NF biocomposite film is highly stable for repeated analysis of ethanol up to five times using single modified electrode. In order to ascertain the reproducibility of the ethanol quantification results, six biocomposite film modified GCEs have been prepared and their electrocatalytic response towards 1.5 M ethanol have been examined through DPV technique. From the DPV results, I_{pa} values of ethanol noticed at all six biocomposite film modified GCEs have been calculated and the relative standard deviation (RSD) is 3.1%. This result reveals the good reproducibility of the biocomposite film for ethanol quantification.

Further, the short term stability of the composite film has also been investigated by 30 min continuous potential cycling (from 0 to −0.5 V) in PBS (figure not shown). We compared the % decrease in back ground current before and after 30 min cycling. The composite film retains 80% back ground current even after 30 min continuous potential cycling which implies that the electrostatic interactions between ADH and TBO are quite stable. In order to ascertain the long term operational stability of the developed biosensor, the ADH/TBO/NF film modified GCE was stored in PBS at 4 °C. For every 12 h, cyclic voltammograms have been recorded at this ADH/TBO/NF film in N_2 saturated PBS with 1.5 M ethanol and 25 mM NAD^+. The corresponding I_{pa} values have been recorded and monitored regularly. The results show that biocomposite film exhibits a stable electrocatalytic response towards ethanol up to 84 h with RSD of 5.4%. The good stability of the biocomposite film could be attributed to the strong electrostatic interactions between the oppositely charged ADH, TBO and NF layers.

The electrocatalysis experiments for selectivity studies have been carried out in various analytes such as methanol, propanol, ascorbic acid, uric acid, dopamine and acetic acid. Where, the concentration of ethanol is kept constant at 1.5 M, and then about 1 mM of each analyte was added. The interference of these analytes during ethanol determination has been calculated by the variation between I_{pa} values of ethanol before and after the addition of analytes at ADH/TBO/NF biocomposite film. These interference values are given as activity (%) in supplementary data (Table S3 of supplementary data). Among these results, the presence of methanol increases the activity (%) of ethanol by 2.09% where as the presence of other analytes decreases the activity (%) of ethanol. These selectivity experimental results reveal that ADH/TBO/NF biocomposite film can be efficiently used as a catalyst for ethanol determination.

Table 1
Electroanalytical results of ethanol determination in real samples using DPV at ADH/TBO/NF biocomposite film modified GCE.

Sample	Ethanol (%)	Added (mM)	Found (mM)	Recovery (%)
A	42	72.4	69.5	95.98
		509.0	492.1	96.56
		818.7	789.2	96.26
B	20.1	34.7	35.4	101.94
		68.0	68.6	100.84
		99.1	96.6	97.36
C	20	558.2	548.1	98.16
		578.4	556.9	96.14
		668.7	667.4	99.81
D	7.5	13.0	12.7	98.16
		37.0	36.1	97.57
		47.5	47.3	99.59

A is Tunnel 88 (premium kaoliang liquor) from Matsu Liquor Factory Industry Co., Ltd., Taiwan, and its labeled composition is 42% ethanol along with sorghum and wheat. B is Jinro from Jinro limited, South Korea, and its labeled composition is 20.1% ethanol along with malt and sweet potato. C is Michiu (rice wine for cooking) from Taiwan, and its labeled composition is 20% ethanol along with rice and salt. D is Boones sangria from E & J Gallo winery, USA, and its labeled composition is 7.5% ethanol along with grape, spice and sugar.

3.8. Determination of ethanol in real samples using DPV

The performance of ADH/TBO/NF biocomposite film has been tested by applying it to the determination of ethanol present in real samples. The technique used for the determination was DPV. In these experiments four different types of real samples were used. They are (Sample A) Tunnel 88 (premium kaoliang liquor) from Matsu liquor factory industry Co., Ltd., Taiwan, and its labeled composition is 42% ethanol along with sorghum and wheat; (Sample B) Jinro from Jinro limited, South Korea, and its labeled composition is 20.1% ethanol along with malt and sweet potato; (Sample C) Michiu (rice wine for cooking) from Taiwan, and its labeled composition is 20% ethanol along with rice and salt; and (Sample D) Boones sangria from E & J Gallo Winery, USA, and its labeled composition is 7.5% ethanol along with grape, spice and sugar. The concentration of ethanol added, found and recovery achieved at the ADH/TBO/NF biocomposite film for above said four samples are given in Table 1. From the electroanalytical results given in Table 1 it is obvious that ADH/TBO/NF biocomposite film is efficient for ethanol detection in real samples.

4. Conclusions

In the present study, a strategy has been employed to develop ADH based biosensor for the determination of ethanol. Attempts have been made to improve the stability of the developed ethanol biosensor through the electrostatic interactions between different films instead of covalent immobilization approach. The electrostatic interactions between the oppositely charged films significantly reduce the leaching of the ADH and thus greatly help to improve the biosensor stability. For the first time, ADH modified GCE surface has been successfully employed for the adsorption of the redox mediator TBO present in the solution. The good electrostatic interactions between the oppositely charged ADH and TBO molecules help to anchor the ADH on GCE surface. We reported

the possible adsorption sites of TBO and NF at ADH both in the presence and absence of NAD^+ using the lowest free energies calculated from their simulation data. The beneficiary aspects of the ADH incorporated biocomposite film rely also on the use of less complex electrode matrices with minimum and simple fabrication steps. Besides, the developed ADH/TBO/NF biocomposite film possesses significant characteristics like high sensitivity, low potential ethanol detection, good repeatability and reproducibility with appreciable operational stability under storage conditions.

Acknowledgements

This work was supported by the National Science Council and the Ministry of Education of Taiwan (Republic of China).

Appendix A. Supplementary data

Supplementary data associated with this article can be found, in the online version, at doi:10.1016/j.talanta.2010.10.058.

References

[1] M. Rocchia, M. Ellena, G. Zeppa, J. Agric. Food Chem. 55 (2007) 5984–5989.
[2] L.D. Mello, L.T. Kubota, Food Chem. 77 (2002) 237–256.
[3] D.J. Caven-Quantrill, A.J. Buglass, J. Chromatogr. A 1117 (2006) 121–131.
[4] R. Vonach, B. Lendl, R. Kellner, J. Chromatogr. A 824 (1998) 159–167.
[5] L. Wu, M. McIntosh, X. Zhang, H. Ju, Talanta 74 (2007) 387–392.
[6] M. Zhou, L. Shang, B. Li, L. Huang, S.J. Dong, Biosens. Bioelectron. 24 (2008) 442–447.
[7] L.V. Shkotova, A.P. Soldatkin, M.V. Gonchar, W. Schuhmann, S.V. Dzyadevych, Mater. Sci. Eng. C 26 (2006) 411–414.
[8] A.M. Azevedo, D.M.F. Prazeres, J.M.S. Cabral, L.P. Fonseca, Biosens. Bioelectron. 21 (2005) 235–247.
[9] Y.V. Rodionov, O.I. Keppen, M.V. Suckhacheva, Appl. Biochem. Microbiol. 38 (2002) 395–396.
[10] I.S. Alpeeva, A. Vilkanauskyte, B. Ngounou, E. Csoregi, I.Y. Sakharov, M. Gonchar, W. Schuhmann, Microchim. Acta 152 (2005) 21–27.
[11] M.M. Barsan, M.A.B. Christopher, Talanta 74 (2008) 1505–1510.
[12] P.C. Pandey, S. Upadhyay, I. Tiwari, V.S. Tripathi, Electroanalysis 13 (2001) 820–825.
[13] Q. Yao, S. Yabuki, F. Mizutani, Sens. Actuators B 65 (2000) 147–149.
[14] Y. Liu, F. Yin, Y. Long, Z. Zhang, S. Yao, J. Colloid Interface Sci. 258 (2003) 75–81.
[15] K. Oshima, T. Nakamura, R. Matsuoka, T. Kuwahara, M. Shimomura, S. Miyauchi, Synth. Met. 152 (2005) 33–36.
[16] C. Jiang, H. Chen, J. Kong, Electrochim. Acta 55 (2009) 142–147.
[17] Y. Motoyama, N. Nakamura, H. Ohno, Electroanalysis 20 (2008) 923–926.
[18] R.T. Kachoosangi, M.M. Musameh, I. Abu-Yousef, J.M. Yousef, S.M. Kanan, L. Xiao, S.G. Davies, A. Russell, R.G. Compton, Anal. Chem. 81 (2009) 435–442.
[19] C. Lee, Y. Tsai, Sens. Actuators B 138 (2009) 518–523.
[20] M. Piao, D. Yang, K. Yoon, S. Lee, S. Choi, Sensors 9 (2009) 1662–1677.
[21] J. Park, H. Yee, K.S. Lee, W. Lee, M. Shin, T. Kim, S. Kim, Anal. Chim. Acta 390 (1999) 83–91.
[22] B. Grundig, G. Wittstock, U. Rudel, B. Strehlitz, J. Electroanal. Chem. 395 (1995) 143–157.
[23] C.O. Schmakel, K.S.V. Santhanam, P.J. Elving, J. Am. Chem. Soc. 97 (1975) 5085.
[24] J. Moiroux, P.J. Elving, J. Electroanal. Chem. 102 (1979) 93.
[25] R. Yuan, S. Kuwabata, H. Yoneyama, Chem. Lett. (1996) 137–138.
[26] J. Razumiene, A. Vilkanauskyte, V. Gureviciene, V. Laurinavicius, N.V. Roznyatovskaya, Y. Ageeva, M.D. Reshetova, A.D. Ryabov, J. Organomet. Chem. 668 (2003) 83–90.
[27] A.S. Santos, A.C. Pereira, N. Duran, L.T. Kubota, Electrochim. Acta 52 (2006) 215–220.
[28] X. Jiang, L. Zhu, D. Yang, X. Mao, Y. Wu, Electroanalysis 21 (2009) 1617–1623.
[29] B.L. Hassler, R.M. Worden, Biosens. Bioelectron. 21 (2006) 2146–2154.
[30] L. Meng, P. Wu, G. Chen, C. Ca, J. Electrochem. Soc. 155 (2008) F231–F236.
[31] P. Du, S. Liu, P. Wu, C. Cai, Electrochim. Acta 53 (2007) 1811–1823.
[32] W. Zhao, J. Xu, H. Chen, Electroanalysis 18 (2006) 1737–1748.
[33] X.Y. Peng, H.Q. Luo, N.B. Li, Microchim. Acta 156 (2007) 297–302.
[34] X. Li, R. Yuan, Y. Chai, L. Zhang, Y. Zhuo, Y. Zhang, J. Biotechnol. 123 (2006) 356–366.
[35] A.C. Perinotto, L. Caseli, C.O. Hayasaka, A. Riul Jr., O.N. Oliveria Jr., V. Zucolotto, Thin Solid Films 516 (2008) 9002–9005.
[36] H. Sund, H. Theorell, Alcohol Dehydrogenases, vol. 7, 2nd ed., Academic Press, London, 1963, pp. 25–83.
[37] W.R. Bowen, S.Y.R. Pugh, N.J.D. Schomburgk, J. Chem. Technol. Biotechnol. 36 (1986) 191–196.
[38] P.A. Prakash, U. Yogeswaran, S.M. Chen, Talanta 78 (2009) 1414–1421.
[39] S.M. Chen, G. Chuang, V.S. Vasantha, J. Electroanal. Chem. 588 (2006) 235–243.
[40] M.A. Rauf, S.M. Qadri, S. Ashraf, K.M. Al-Mansoori, Chem. Eng. J. 150 (2009) 90–95.
[41] E. Laviron, J. Electroanal. Chem. 101 (1979) 19–28.
[42] M. Weissmann, S. Baranton, J. Clacens, C. Coutanceau, Carbon 48 (2010) 2755–2764.
[43] W. Schuhmann, H. Zimmermann, K. Habermuller, V. Laurinavicius, Faraday Discuss 116 (2000) 245–255.
[44] E. Katz, I. Willner, Electroanalysis 15 (2003) 913–947.
[45] H.O. Finklea, D.A. Snider, J. Fedyk, Langmuir 9 (1993) 3660–3667.
[46] C.P. Andrieux, O. Haas, J.M. Savgant, J. Am. Chem. Soc. 108 (1986) 8175–8182.